ACADEMIC PRESS

Available online at www.sciencedirect.com

SCIENCE DIRECT®

Journal of Magnetic Resonance 163 (2003) 38–45

JMR Journal of Magnetic Resonance

www.elsevier.com/locate/jmr

Two-dimensional imaging with a single-sided NMR probe

F. Casanova and B. Blümich*

Institute for Technical Chemistry and Macromolecular Chemistry, Aachen University of Technology, RWTH, Aachen D-52056, Germany

Received 20 November 2002; revised 26 February 2003

Abstract

A new low field unilateral NMR sensor equipped with a two-dimensional gradient coil system was built. A new NMR-MOUSE concept using a simple bar magnet instead of the classical U-shaped geometry was used to produce magnetic field profiles comparatively homogeneous in extended lateral planes defining a suitable field of view for 2D spatial localization. Slice selection along the depth direction is obtained by means of the highly constant static magnetic field gradient produced by this magnet geometry. Implementing a two-dimensional phase-encoding imaging method 2D cross sections of objects were obtained with high spatial resolution. By retuning the probe it was possible to change the depth of the selected slice obtaining a 3D imaging method. The details of the construction of the new device are presented together with imaging tests to show the quality of space encoding.

Keywords: MRI; Unilateral NMR; Mobile probes; NMR-MOUSE

1. Introduction

The application range of unilateral NMR has experienced considerable expansion during the last years [1,2]. The use of single-sided probes is not limited by the object size making NMR a truly non-invasive method suitable for near surface studies of arbitrarily large objects. Characterization of fluids, polymers, and porous media can be done in situ by measuring relaxation times, self-diffusion coefficients, and multi-quantum effects [3–6]. Also the analysis can be made quantitative by calibrating the signal intensity using reference samples.

A simple design of a unilateral sensor is the so-called NMR-MOUSE [7] (Nuclear Magnetic Resonance Mobile Universal Surface Explorer) which requires two permanent magnets with anti-parallel polarization positioned on an iron yoke forming a magnet in the classical horseshoe geometry (U-shaped magnet) to generate the static magnetic field, and a radiofrequency (RF) coil positioned in the air gap between magnets used for excitation and detection of the NMR signal.

To characterize heterogeneous specimens NMR imaging has been demonstrated to be of great assistance [8,9]. Lateral spatial resolution was previously obtained with the NMR-MOUSE simply by lateral displacement of the probe [7]; but besides low precision in positioning the sensor low spatial resolution is obtained depending on the shape of the sensitive volume defined by both B_0 and B_1 spatial distributions. Depth selectivity into the object can also be obtained by retuning the resonance frequency of the probe. Although the shape of the static magnetic field is well known, it is highly inhomogeneous introducing severe problems for slice selection along the depth direction since the sensitive volume is not flat at all [10].

Recently Prado et al. [11] have shown that it is possible to incorporate spatial resolution along one spatial coordinate by superimposing a pulsed magnetic field gradient and using a pure spin-echo phase-encoding method (single-point imaging). A gradient coil system was mounted in the gap between the magnets of a U-Shaped NMR-MOUSE to apply pulsed magnetic fields with a principal gradient along the direction x of the gap. This axis was selected as the imaging direction because the magnet geometry defines a sensitive volume which, at the surface of the magnets, is of the order of 10 mm along x and 2 mm along y. Using single point imaging a spatial resolution of the order of a few hundred microns along the gap direction was obtained.

* Corresponding author. Fax: +49-241-8888-185.
E-mail address: bluemich@mc.rwth-aachen.de (B. Blümich).

1090-7807/03/$ - see front matter
doi:10.1016/S1090-7807(03)00123-X

The aim of this work is to demonstrate that cross sectional images can be obtained implementing a pure two-dimensional phase encoding technique in a single-sided sensor with an appropriate design. An extension of the 1D technique to a 2D version requires the design of a suitable gradient coil system and principally a magnet geometry producing a sensitive volume extended in two directions to define a useful plane of view. The magnet geometry used in this work is a recently proposed one that uses a single bar-shaped magnet where the magnetic field lines emanate perpendicular from the pole face of the permanent magnet (z-direction), and the RF surface coil is located on one of the pole faces [12]. The principal magnetic field gradient component is also along the z direction (depth direction) defining rather flat slices of constant frequency and a field of view that can be considered symmetric in both perpendicular x and y directions. We mounted an appropriate gradient coil system to produce the two perpendicular gradient fields along both x and y directions, and using a two-dimensional spin-echo phase encoding technique 2D spatial localization was obtained. A combination of the 2D phase encoding technique with the natural slice selection along the depth direction can be used to obtain 3D spatial resolution just by retuning the probe to different frequencies.

In the following sections complete descriptions are given of the imaging method and of the device built to obtain 2D space encoding. Results of imaging experiments are presented which show the quality of the spatial localization and of slice selection. Finally a 2D image is presented which demonstrate the performance of the device and the technique.

2. Method

Fig. 1 shows the two-dimensional pulse sequence for phase encoding by the spin echo method used to measure a cross section of an object. The method is similar to the proposed by Godward et al. [13] and used to produce images of planar samples in the stray field of superconducting magnets. Due to the presence of a highly inhomogeneous static magnetic field only a phase encoding spin echo method can be used. A Hahn echo sequence is applied to refocus the magnetization spread introduced by the static field inhomogeneities while the pulsed gradients modulate the phase of the echo according to the in-plane position of the spins.

To obtain the best performance for space encoding the gradient pulses must be applied simultaneously after the second RF pulse, then shortest echo times can be achieved. Due to experimental limitations it was not possible for us to simultaneously pulse the gradients, and two alternatives were analyzed. In the first case the pulses can be applied in succession with the necessity of a long echo time determined by the sum of the encoding times t_x and t_y, which results in signal loss from transverse relaxation. The second one is to apply one gradient pulse in each free evolution interval, as shown in Fig. 1, at expenses of introducing possible distortions in the phase encoding by the second RF pulse. In this work the second variant was chosen after verifying, that no artifacts were induced by the flip angle distribution of the refocusing pulse.

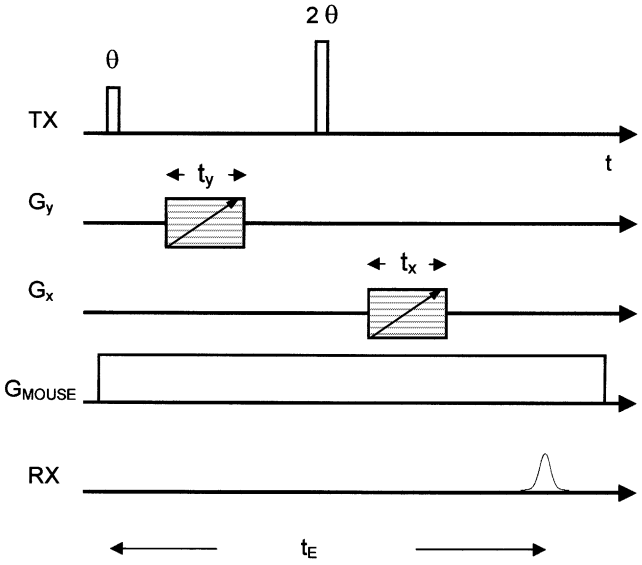

Fig. 1. Spin echo sequence for pure 2D phase encoding spin echo sequence used to obtain 2D space encoding in the presence of a strong static field gradient. A Hahn echo sequence is applied with an echo time t_E. Both RF pulses have the same length to arrive at similar excitation bandwidths, but different amplitudes to fulfill the nominal $\pi/2$ and π flip angles. Two gradient pulses are applied with encoding times t_x and t_y, one in each free evolution interval of the sequence.

To arrive at the same spectral excitation bandwidth for both RF pulses (nominal $\pi/2$ and π pulses) the lengths of them were equal, but their amplitudes were adjusted for maximum echo amplitude. Although the RF pulses are not soft and because of the presence of a strong static magnetic field gradient a thin slice perpendicular to the gradient direction is selected by the pulse sequence fully equivalent to the well-known imaging methods [9,14].

3. Experimental

A drawing of the bar magnet NMR-MOUSE equipped with the gradient coil system built for this work is depicted in Fig. 2. In the following, a complete description of the magnetic field profile, the geometry of the RF coil, and the configuration of the gradient coil system are presented.

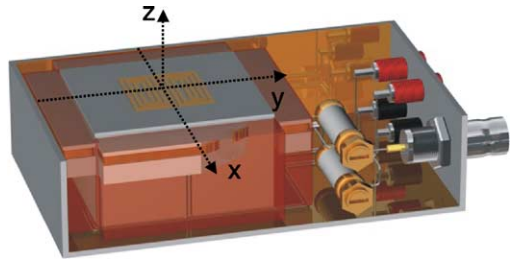

Fig. 2. Drawing of the bar magnet NMR-MOUSE equipped with the gradient coil system to apply pulsed gradient fields with gradients along x and y. The rectangular magnet block $40 \times 45 \times 20$ mm^3 produces a magnetic field strength of 0.44 T at the surface. On one face of the magnet a Fig. 8 RF coil is positioned to produce a B_1 field which in the center of the magnet has a principal component along the y direction. At each side of the magnet four rectangular coils 45×8 mm^2 are positioned and driven in pairs to generate the gradient fields.

3.1. Static magnetic field characteristics

The new MOUSE concept uses a single rectangular block NeFeB permanent magnet with dimensions $45 \times 40 \times 20$ mm^3 which provides a static magnetic field along the direction perpendicular to the largest surface of the magnet (Fig. 2). To probe the spatial variation of the static magnetic field the three components of $\mathbf{B}_0$ were scanned in the complete region near the pole face of the magnet using a LakeShore 420 Hall probe. Fig. 3 shows the spatial dependence of B_{0x}, B_{0y}, and B_{0z} along the x-axis for $y = 0$, and $z = 3$ mm, where the axes directions are shown in Fig. 2. The origin was set in the center of the pole face and $z = 0$ on the surface of the magnet. As expected for this magnet geometry, B_{0z} is the principal component and remains almost constant along the scanned region, B_{0x} and B_{0y} are nearly zero in the center of the magnet and, while B_{0x} changes linearly with the position, B_{0y} remains close to zero. Also in the same plot

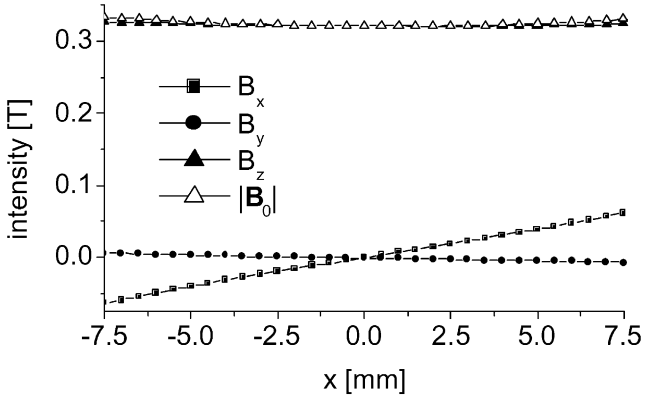

Fig. 3. Spatial dependence of the three components of $\mathbf{B}_0$ scanned along the x direction and plotted together with the magnitude of the magnetic field computed from the measured values. It can be observed that in a region of 1 cm in the center of the magnet the magnitude of $\mathbf{B}_0$ is approximately equal to that of B_{0z}.

it is shown the value of the total magnetic field B_0 is shown as computed from the measured components. In a region of 1 cm in the center of the magnet pole face the value of B_{0z} closely approximates B_0, demonstrating that the magnetic field can be considered to be parallel to the z-axis. In the following and for the sake of experimental simplicity the shape of the sensitive volume is determined measuring only the spatial dependence of the B_{0z} component.

In Fig. 4a the variation of B_{0z} along the x–z plane at $y = 0$ is plotted. The position $z = 0$ was chosen at the surface of the magnet but the scanned region starts from $z = 2$ mm leaving this 2 mm space for positioning the RF coil. Although the field intensity is not perfectly symmetric around $x = 0$ due to the usual imperfections observed in this kind of magnets such deviations are tolerable. We can see that the magnetic field possesses a strong gradient along the z axis while the variation along the x direction is smooth enough to define a rather flat sensitive volume. The levels shown in the plot are separated by 300 kHz corresponding to the excitation bandwidth when RF pulses of 3 μs length are applied. It can be observed that the spacing of the lines (thickness of the excited slice) is about 0.4 mm and almost parallel to the x direction so that the slice selected for a given frequency is quite flat in a field of view of 10 mm along the x direction. This shape of the excited volume is of great advantage for slice selection along the z axis which can be achieved just by retuning the probe. It must be noticed the flatness of the selected slice depends on the dimension of the excited volume along both x and y directions, obtaining the best results when operating as close as possible in the center. The selection of a desired region along the x and y axes can only be made by choosing a suitable RF coil dimension, which must be small enough to assure the desired quality in the slice selection along z.

In Fig. 4b the B_{0z} field component along a x–y plane is shown at $z = 2$ mm. This map shows how flat the shape of the sensitive volume is in the 2D plane and illustrates the symmetry of the field along x and y directions. Finally in Fig. 4c the B_{0z} intensity is plotted as a function of z. The variation of the magnetic field is highly linear with a gradient value of 16.6 T/m.

3.2. Radiofrequency coil

An appropriate RF coil to produce a $\mathbf{B}_1$ field with a principal component perpendicular to $\mathbf{B}_0$ was etched on a standard printed circuit board. This coil has the geometry of Fig. 8 [15], and the dimensions and shape are shown in Fig. 5a. An important characteristic of this design lies in the external noise cancellation important in an open devise [16]. The complete RF field distribution of the component B_{1xy} perpendicular to $\mathbf{B}_0$ was calculated using the Biot–Savart law and the result is

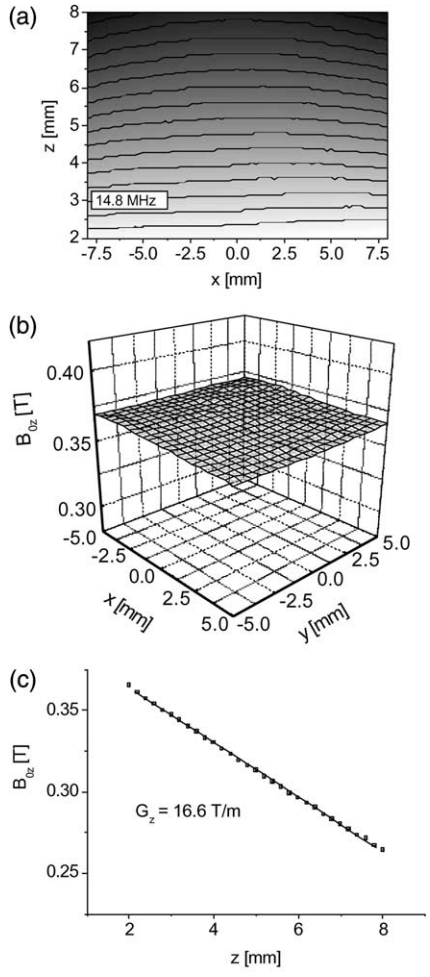

Fig. 4. Component B_{0z} of the magnetic field measured using a LakesShore 420 Hall probe with a resolution of 0.01 mT. (a) Map of the B_{0z} component in the x–z plane centered at $y = 0$. The grey scale shows how the field decreases with the distance from the magnet. The solid lines mark frequency decrements of 300 kHz for ^{1}H, and the one at 3 mm from the magnet (1 mm depth) is labeled with its correspondent frequency value, 14.8 MHz. They serve to visualize the thickness and the flatness of the slice selected by a 3 μs long RF pulse. A slice thickness of 0.4 mm is excited and the position of it along z changes slightly in the region of interest covering 1 cm from center at both sides. (b) Map of the B_{0z} component in the x–y plane center at $z = 2$ mm. The symmetry of the magnetic field defines a square sensitive volume. (c) Dependence of B_{0z} along the z-axis. The gradient of the static filed is rather constant with a value of 16.6 T/m. It ensures a uniform slice thickness as a function of z.

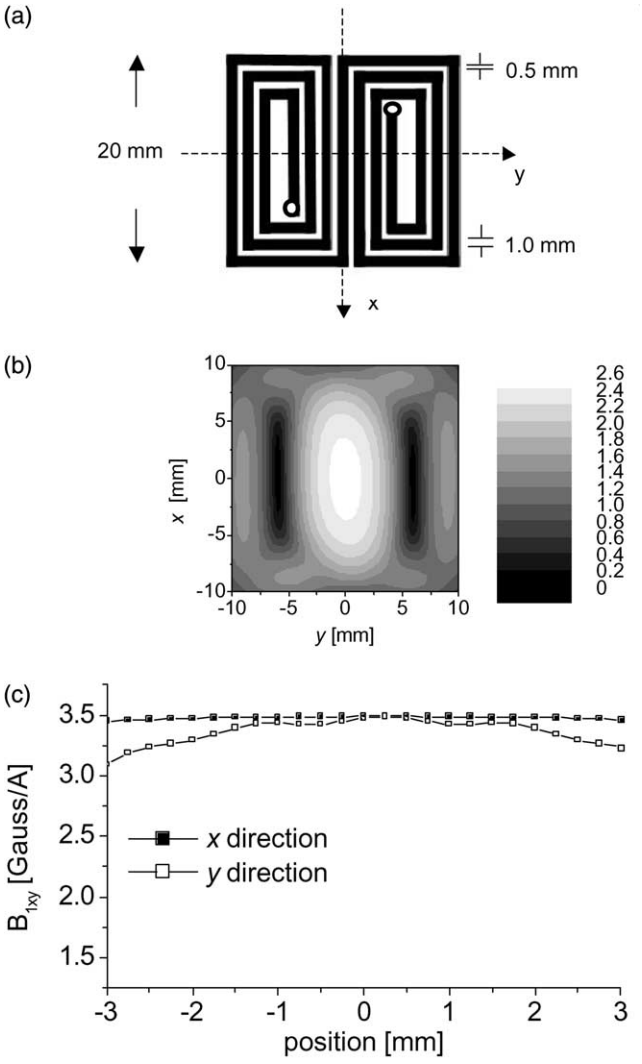

Fig. 5. (a) Radiofrequency coil with a Fig. 8 geometry printed on a circuit board 2 mm tick, which is positioned on the top of the magnet. (b) Magnetic field component B_{1xy} calculated for a distance of 1 mm from the coil surface. The scale is in Gauss/Ampere and the map shows the field distribution when a current of 1 A is applied. The sensitive region in the center of the coil appears bright. (c) Dependence of B_{1xy} along the x and y directions. The intensity along x is constant and the intensity along y changes by less than 10% in the region of interest. Although the field has a strong gradient along z it is possible to define uniform RF field amplitude inside each selected slice.

shown in Fig. 5b. In this device the RF coil is positioned at 2 mm from a copper sheet that covers the block magnet and reduces the acoustic ringing [15]. To check that the RF field distribution is not appreciably distorted by the eddy currents generated in the metallic surrounding the NMR echo-signal intensity of a voxel of 1 mm^3 was scanned in the region above the RF coil. Using the signal intensity to measure the B_1 intensity the behavior shown in Fig. 5b was reproduced. For a more accurate determination of the $\mathbf{B}_1$ field distribution eddy currents induced in the copper film that shield the magnet must be considered in a numerical calculation, but this analysis is out of the scope of the present work. When this coil is positioned on the surface of the magnet it produces a B_1 field almost constant in a region of 6×8 mm^2 centered in the middle of the magnet.

Fig. 5c shows the dependence of B_{1xy} along the x and y axes. Along the x direction the RF field is constant and along y it has a small variation of about 10% which for our purposes is acceptable and made possible to define a rather uniform flip angle inside a flat selected slice.

3.3. 2D gradient coil system

To produce pulsed gradients along the x and y directions four rectangular coils working in pairs were mounted at each side of the permanent magnet as shown in Fig. 2. Each coil has a 45 mm × 8 mm cross-section and 20 turns. The coils on opposite sides were connected in series producing an anti-parallel field changing from positive to negative values along each respective direction. The z component of the magnetic field produced by each pair was calculated in the region of interest. Fig. 6 shows the variation of the gradient field B_z along the x and y axes, respectively. The spatial variation is linear, and the slopes define the gradient amplitudes along each direction. As the separation between each coil pair is not the same, the gradient along x is stronger than the gradient along y.

The gradient coils were shielded with a cover made from a copper sheet to reduce the coupling between gradient and the RF coils, as well as the noise coming from the power amplifiers. Two Techron amplifiers model 7541 were used to drive the coils delivering a maximum voltage of 60 V and a maximum current of 20 A. In our case the resistance of each coil pair is 0.8 Ω and the maximum gradient is limited by the maximum current available which is 0.40 and 0.24 T/m in each case.

The rise time of these coils was measured by detecting the voltage induced during the application of the gradient current pulses, it is around 50 μs. Although not used in this work pre emphasis current modulations can be superimposed to the rectangular shape of the gradient pulses in order to decrease the transients periods that limited the usable echo times.

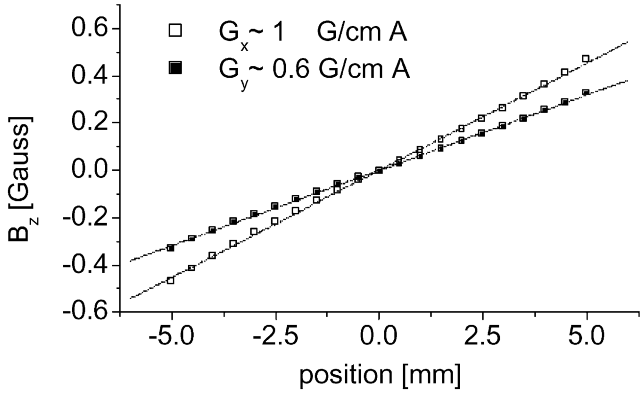

Fig. 6. Spatial dependence of the gradient field intensity produced by each pair of coils. In a 1 cm region the field variation is linear for both directions. The gradient along each direction has a different value because of the different separations between the coils determined by the rectangular shape of the magnet.

4. Results

To determine the quality of the space encoding 1D images were obtained along both coordinates x and y. A simple object geometry composed of two strips of natural rubber 2.5 mm and 1.5 mm wide, 8 mm long, and separated by 1 mm, was chosen to estimate possible distortions along each axis. The thickness of the strips was 2 mm and the probe was tuned at 14.8 MHz selecting a slice at 1 mm depth from the RF coil surface. The longitudinal relaxation time T_1 of this sample is about 20 ms, and a recycling delay of 30 ms was used for fast averaging. The 1D imaging method proposed by Prado was used [11]. The echo time was set to 0.7 ms, and the gradient pulse was switched after the second RF pulse. The gradient amplitude was increased in 21 steps, sampling the **k** space from negative to positive values. The maximum voltage of the amplifier was kept constant, and the field of view was adjusted by changing the encoding times t_x and t_y in each case. Fig. 7a shows a 1D image along the x axis obtained by applying an encoding time of 200 μs and 1000 scans. The total time needed to obtain the image was about 10 min at a spatial resolution of 250 μm. In Fig. 7b a 1D image of the same object but with the structure aligned along the y direction is shown. For this case the encoding time was set to 300 μs to compensate for the fact that the value of G_y is smaller than G_x. Both images were scaled using the known dimensions of the object, and it can be observed they have similar quality showing the symmetry in the field of view and proving that this design is appropriated for the reconstruction of two-dimensional images.

It was anticipated that for the implementation of the 2D imaging method one of the gradient pulses must be applied during the first free evolution interval. To check the equivalence of applying an encoding interval preceding the refocusing pulse another 1D imaging experiment was done. A G_y gradient pulse lasting 300 μs was applied using an echo time of 0.7 ms. Fig. 7c shows the 1D image obtained using the same experimental parameters as for the previous experiment. Scaling the image from the dimension of the object a slightly bigger field of view compared with the one of the experiment shown in Fig. 7b is obtained. The small reduction on the effective gradient pulse length is due to a spurious refocusing of the gradient field as consequence of a long falling time of the pulsed field, which is different from zero when the refocusing pulse is applied. Nevertheless, no distortions can be observed in the image, which perfectly reproduces the object structure. The interval between the RF pulses was purposely set comparable to the gradient pulse length to illustrate the problem, and in a correct experiment a long enough echo time must be chosen depending on the falling time of the pulsed field gradient. This experiment demonstrates that gradient pulses can be applied before or after the refocusing pulse

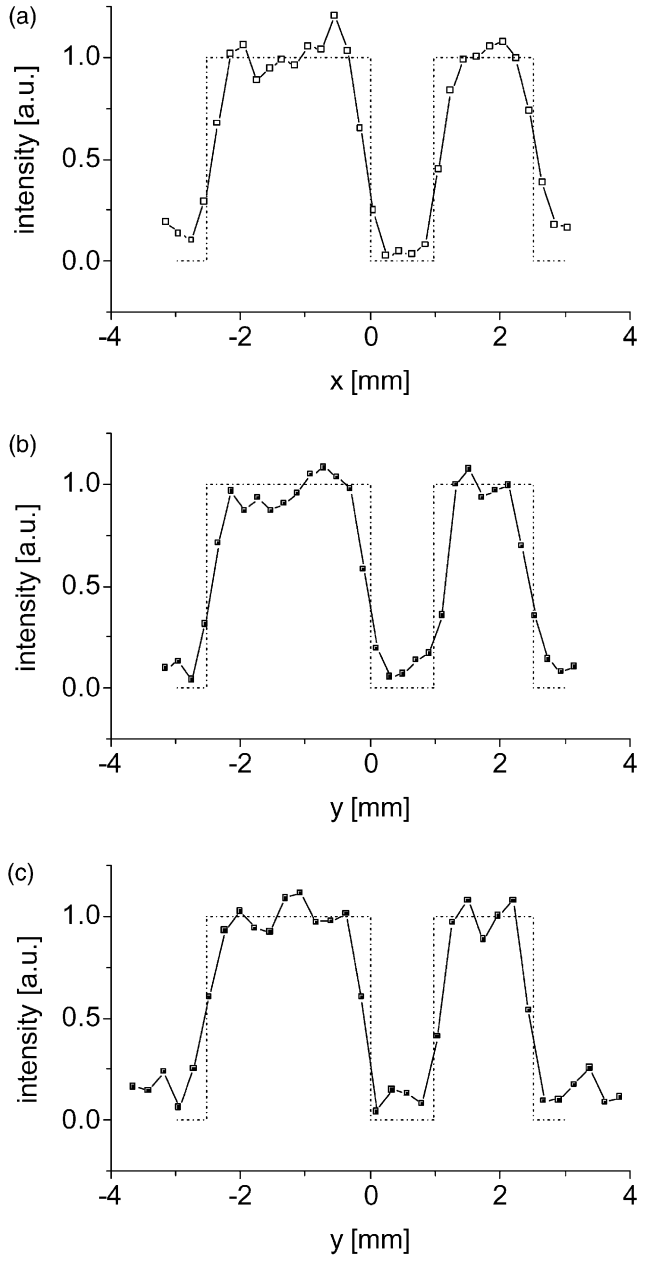

Fig. 7. One-dimensional images obtained along both x and y directions showing the symmetry of the space encoding along both axes. A simple object consisting of two rubber strips with different widths (2.5 mm and 1.5 mm) and separated by 1 mm was imaged. In all plots the object profile was superimposed to the images in order to compare it with the experimental results. For all the experiments the power supplies driving the gradient coils were set at the same voltage, producing different gradient amplitudes along the x and y directions. The **k** space was sampled using 21 gradient steps and a zero filling up to 32 points was done previous to Fourier transformation. (a) 1D image obtained orienting the object structure along the x axis. A field of view (FoV) of 6.5 mm was obtained using a gradient pulse length of 200 μs, and $G_{x,\max} = 0.18$ T/m. (b) 1D image with the object structure along the y axis. A FoV of 6.5 mm was obtained using a gradient pulse length of 300 μs, and $G_{y,\max} = 0.12$ T/m. (c) 1D image with the object structure along the y axis but applying the gradient pulse in the first evolution interval of the Hahn-echo sequence. The effective gradient intensity is reduced to $G_{y,\max} = 0.095$ T/m because of the failing time of the gradient field pulse past the refocusing RF pulse. In this case the FoV is 7.5 mm.

so that the pulse sequence of Fig. 1 can be implemented. It can also be used to reduce the echo time by one half in 1D experiments where the gradient pulse can be split in two and applied with opposite polarities one before and the second after the refocusing pulse to obtain the same encoding time.

To test the quality of the slice selection by choice of the resonance frequency an object with a fine internal structure was chosen. A rubber band 2 mm thick and 5 mm long, which contained nylon fibbers aligned parallel one to each other was positioned above the probe with the fibers perpendicular to the x axis as shown in Fig. 8a.

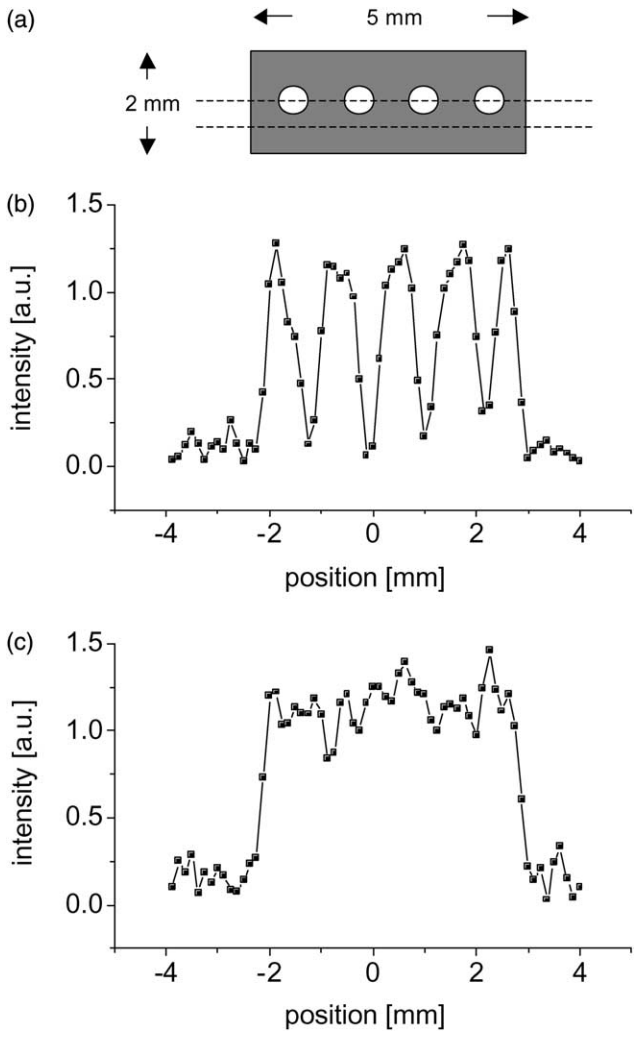

Fig. 8. One-dimensional images obtained along the x-axis for different slices positions selected by retuning the probe to different frequencies. The gradient intensity was increased in 41 steps sampling the **k** space from negative to positive values, and a zero filling up to 64 points was used. (a) A 5 mm wide and 2 mm thick rubber sheet structure containing four nylon fibers was positioned on the device with the fibers perpendicular to the x direction to test the quality of the slice selection along z. (b) 1D image obtained at 14.8 MHz corresponding to a slice position at 1 mm depth, exactly where the fibers. (c) 1D image obtained at 15.2 MHz corresponding to a slice position at 0.6 mm underneath the fibers.

The resonance circuit was tuned to two different frequencies, the first one to 14.8 MHz was set to select a slice at 1 mm from the probe surface exactly where the fibbers are and the second one to 15.2 MHz was set to select a slice 0.6 mm underneath the center of the fibers where there is a homogeneous rubber distribution. Using an echo time of 500 μs two gradient pulses 200 μs long were applied before and after the refocusing pulse. It duplicates the effective gradient pulse length used in the experiment of Fig. 7a, but the same field of view was set increasing the gradient amplitude in 41 steps. In this way a spatial resolution better than 150 μm was obtained. In Figs. 8b and c the 1D projections measured at these two depths are shown. Using a recycling delay of 30 ms and 3000 scans a measuring time of 1 h was needed per experiment. The results show that the static gradient along the z-axis can be used for slice selection and by combining it with pulsed gradients along the x or y direction 3D images can be obtained.

Finally, a x–y slice was measured using the 2D phase encoding echo sequence of Fig. 1. A 75 μs long gradient pulse was applied along the y-axis and a 50 μs long gradient pulse along the x direction. 17 gradient increment steps were used in each direction defining a field of view of about 16 mm in both directions and a spatial resolution of about 1 mm. Fig. 9a depicts a drawing of the object. It is a capital letter 'F' cut from a sheet of natural rubber with the dimensions specified in the figure. Fig. 9b shows the cross section obtained by tuning the probe at 14.8 MHz (1 mm from the RF coil). One hundred and fifty scans were averaged with a recycling delay of 30 ms determining the experimental time necessary to obtain the complete 2D matrix to 1 h 15 min. One can clearly see the geometry of the object without appreciable distortions.

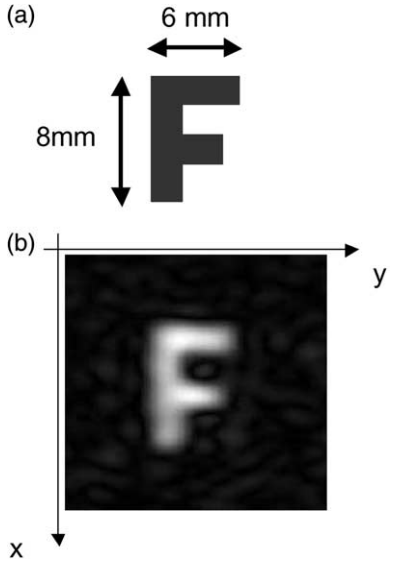

Fig. 9. 2D imaging. (a) Object geometry used to test the two-dimensional spatial localization technique. A capital "F" letter was cut from a sheet of natural rubber and positioned in the center of the RF coil. (b) Cross section obtained with 1 mm spatial resolution in an experimental time of 1 h 15 min. The intensity of both gradients was increased in 17 steps sampling the complete **k** space and a zero filling up to 64 points along each direction was used.

5. Conclusion

A new single-sided NMR sensor equipped with a gradient coil system to produce pulsed gradients along two perpendicular directions was built. Due to the continuous presence of a strong static gradient along the static magnetic field direction a single point spin-echo imaging method was used to obtain 2D images encoding the spatial information in the phase of the echo signal. To provide the static magnetic field a simple permanent magnet in the shape of a rectangular block was used instead of the conventional U-shaped geometry. This bar magnet provides a symmetric field of view along the x and y axes suitable for 2D spatial localization and a rather flat sensitive volume defined by a highly constant gradient along the z axis suitable for slice selection. The high quality of space encoding and the time necessary to measure 1D and 2D cross sections demonstrate the promising potential of the method to characterize heterogeneous samples not only through the image intensity but also by locally measuring relaxation times maps. We are currently exploring multi-echo methods to acquire a set of relaxation weighted 2D images in a single experiment to either compute spatially resolved T_2 maps or to add the signals from different echoes to improve the signal-to-noise obtained in each scan.

Acknowledgments

F.C. thanks the Alexander von Humboldt Foundation for a Research Scientist Fellowship. Support of this project by the DFG Forschergruppe FOR333 Surface NMR of Elastomers and Biological Tissue is gratefully acknowledged.

References

[1] R.L. Kleinberg, A. Sezginer, D.D. Griffin, M. Fukuhara, Novel NMR apparatus for investigating an external sample, J. Magn. Reson. 97 (1992) 466–485.

[2] G.A. Matzkanin, A review of non-destructive characterization of composites using NMR, in: P. Höller, V. Hauck, C.O. Rutud, R.E. Green (Eds.), Nondestructive Characterization of Materials, Springer, Berlin, 1998, p. 655.

[3] M.D. Hürlimann, D.D. Griffin, Spin dynamics of Carr–Purcel–Meibohm–Gill-like sequences in grossly inhomogeneous B_0 and B_1 fields and applications to NMR well logging, J. Magn. Reson. 143 (2000) 120–135.
[4] G. Zimmer, A. Guthausen, B. Blümich, Characterization of cross-link density in technical elastomers by the NMR-MOUSE, Solid State Nucl. Magn. Reson. 12 (1998) 183–190.
[5] A. Guthausen, G. Zimmer, P. Blümler, B. Blümich, Analysis polymer materials by the NMR-MOUSE, J. Magn. Reson. 130 (1998) 1–7.
[6] A. Wiesmath, C. Filip, D.E. Demco, B. Blümich, Double-quantum-filtered NMR signals in inhomogeneous magnetic fields, J. Magn. Reson. 149 (2001) 258–263.
[7] G. Eidmann, R. Salvelsberg, P. Blümler, B. Blümich, The NMR-MOUSE, a mobile universal surface explorer, J. Magn. Reson. A 122 (1996) 104–109.
[8] J.B. Miller, NMR imaging of materials, Prog. Nucl. Magn. Reson. Spectrosc. 33 (1998) 273–308.
[9] B. Blümich, NMR Imaging of Materials, Oxford University Press, Oxford, 2000.
[10] F. Balibanu, K. Hailu, R. Eymael, D.E. Demco, B. Blümich, Nuclear magnetic resonance in inhomogeneous magnetic fields, J. Magn. Reson. 145 (2000) 246–258.
[11] P. Prado, B. Blümich, U. Schmitz, One-dimensional imaging with a palm-size probe, J. Magn. Reson. 144 (2000) 200–206.
[12] B. Blümich, V. Anferov, S. Anferova, M. Klein, R. Fechete, M. Adams, F. Casanova, A simple NMR-MOUSE with a bar magnet, Magn. Reson. Eng. 15 (4) (2002) 255–261.
[13] J. Godward, E. Ciampi, M. Cifelli, P.J. McDonald, Multidimensional imaging using combined stray field and pulsed gradients, J. Magn. Reson. 155 (2002) 92–99.
[14] P.T. Callaghan, Principle of Nuclear Magnetic Resonance Microscopy, Clarendon Press, Oxford, 1991.
[15] S. Anferova, V. Anferov, M. Adams, P. Blümer, N. Routley, K. Hailu, K. Kupferschläger, M. Mallet, G. Schroeder, S. Sharma, B. Blümich, Construction of the NMR-MOUSE with short dead time, Magn. Reson. Eng. 15 (2002) 15–22.
[16] B.H. Suits, A.N. Garroway, J.B. Miller, Noise-immune coil for unshielded magnetic resonance measurements, J. Magn. Reson. 131 (1998) 154–158.